Chapter 26
Magneto-Optical Functionalities in Cyano-Bridged Bimetal Assemblies and Metal-Oxide Nanomaterials

Shin-ichi Ohkoshi

26.1 Introduction

Today, I am going to talk about magneto-optical functionalities in cyano-bridged bimetal assemblies and metal-oxide nanoparticles. I have only short time to talk, so I would like to focus on our laboratory work, i.e., magneto-optical functionalities in cyano-bridged metal assemblies in these two compounds of $Fe_2[Nb(CN)_8] \cdot (4\text{-pyridinealdoxime})_8 \cdot 2H_2O$ and $Fe_2[Nb(CN)_8] \cdot (4\text{-bromopyridine})_8 \cdot 2H_2O$.

26.2 Light-Induced Spin-Crossover Magnet

Our laboratory has prepared of several families of magnetic materials based on cyano-bridged metal assemblies using metal complexes [1–9]. Until now, we have demonstrated several types of functionalities as shown in Fig. 26.1. For example, light-induced phase transition behavior of photomagnetism [2,3], electric field-induced phase transition in a magnetic material [4], and a coupling effect between spin and ionic conductivity [5]. Furthermore, we demonstrated humidity-sensitive magnetism [6] and transparent magnetic films. These features are based on metal complexes. Furthermore, we study metal-oxide nanoparticles [10-12]. For example, recently we demonstrated light-induced metal-semiconductor phase transition [10]and hard-magnetic ferrite with huge coercivity [11,12]. I would like to talk about these two topics.

S. Ohkoshi (✉)
Department of Chemistry, School of Science, The University of Tokyo, 7-3-1 Hongo, Bunkyo-ku, Tokyo 113-0033, Japan
e-mail: ohkoshi@chem.s.u-tokyo.ac.jp

K. Yamanouchi (ed.), *Progress in Photon Science*, Springer Series in Chemical Physics 115, DOI 10.1007/978-3-319-52431-3_26

To demonstrate photomagnetism in the material, we focused on the Light-induced excited spin state trapping (LIESST) effect (Fig. 26.2). The LIESST effect is light-induced excited spin-state trapping effect. This effect is very familiar in the field

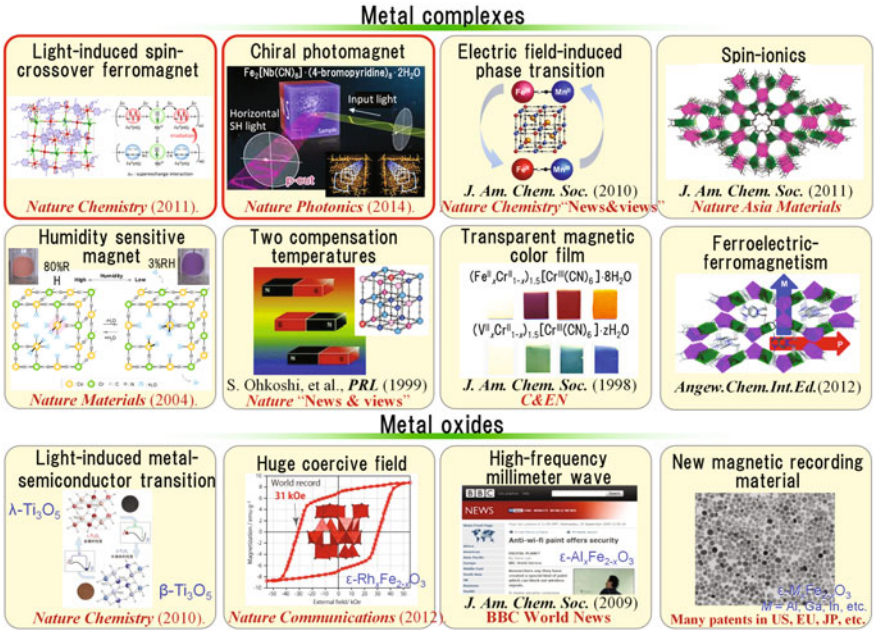

Fig. 26.1 Background researchs on metal complexes and metal oxides

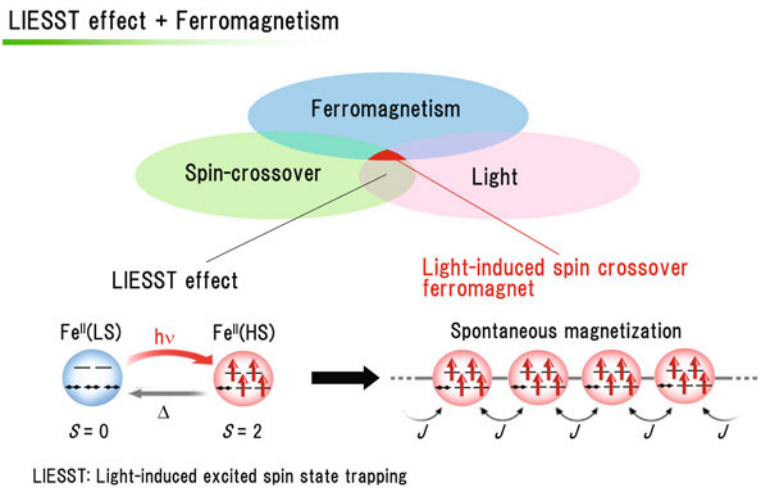

Fig. 26.2 Concept of combining LIESST effect and light-induced ferromagnet

of metal-complex and coordination chemistry. Spin-crossover is the change between iron low-spin and iron high-spin caused by stimuli, for example, light-irradiation. In this case, light irradiation changes the material's property due to the LIESST effect, or simply, photo-induced spin-crossover behavior.

If ferromagnetism is coupled with this property, we can image light-induced spin-crossover ferromagnetism, and spontaneous magnetization is expected to be caused by light-irradiation. This idea is very simple—I think that many scientists considered this simple idea—but before this work, nobody succeeded in observing this phenomenon. The reason is because, in this LIESST effect, the metal cation shows a very large volume change of 5 or 10%. Furthermore, the superexhange interaction between these two paramagnetic species depends on the distance between the metal cations. In the case of a spin crossover metal complex, the super-exchange interaction is very weak, and therefore, spontaneous magnetization cannot be observed.

According to this scenario, we considered demonstrating a light-induced spin-crossover magnetiztion using this material (Fig. 26.3). This material consists of iron and octacyanoniobate with 4-pyridinealdoxime. This material is prepared by mixing these reagents. Iron is coordinated to four nitrogen atoms of 4-pyridinealdoxime and two nitrogen atoms of cyano groups of octacyanoniobate. It has a three-dimensional complicated crystal structure.

We measured the magnetic property of this material (see Fig. 26.4). You can see that, at room temperature and higher temperatures, the magnetic property is derived from iron (II) high-spin and niobium paramagnetic spin. However, with decreasing temperature, magnetization drops abruptly at 130 K. In this low-temperature phase,

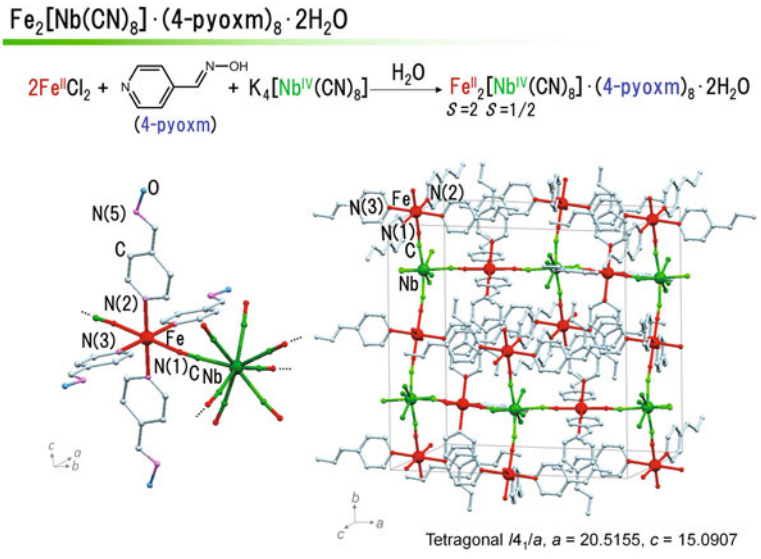

Fig. 26.3 Crystal structure of $Fe_2[Nb(CN)_8] \cdot (4\text{-pyoxm})_8 \cdot 2H_2O$

about 80% of the iron ion is converted from high-spin to low-spin. The iron in the low-temperature phase is basically in the low-spin state. This spin-crossover behavior was also confirmed by Mössbauer spectroscopy and low temperature UV-vis spectroscopy.

Next, we irradiated light onto the sample (Fig. 26.5). Before light irradiation, this material based on iron(II) low-spin and niobium does not show a long-range magnetic ordering, but, by light irradiation, high-spin state is induced, and then a spontaneous magnetization is observed. The Curie temperature is 20 K. At the same time, a

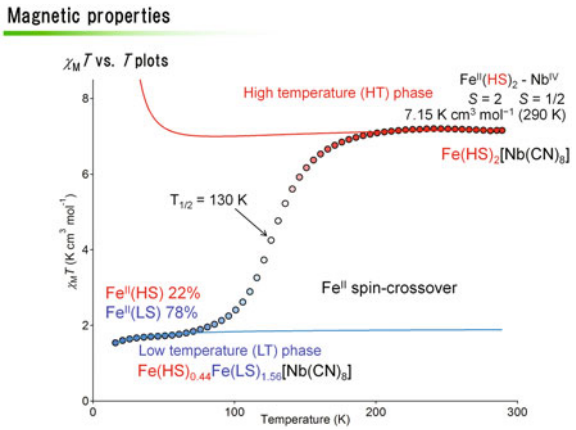

Fig. 26.4 Spin-crossover phenomenon in $Fe_2[Nb(CN)_8] \cdot (4\text{-pyoxm})_8 \cdot 2H_2O$ observed by magnetic measurements

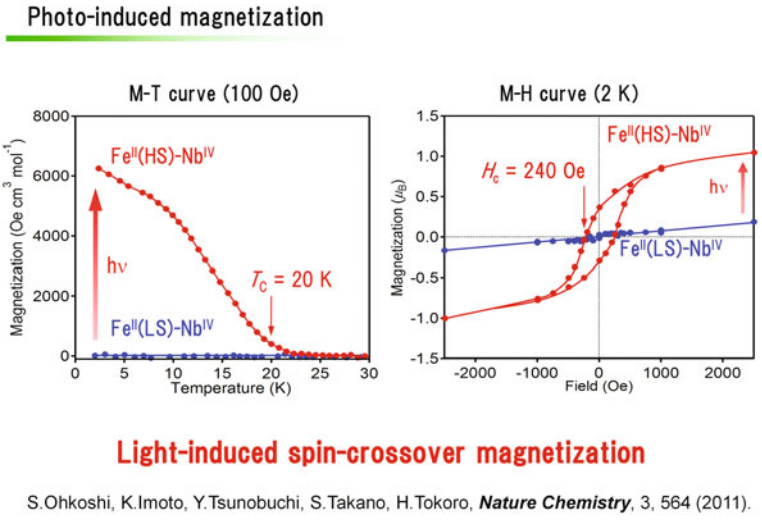

Fig. 26.5 Light-induced spin-crossover magnetization in $Fe_2[Nb(CN)_8] \cdot (4\text{-pyoxm})_8 \cdot 2H_2O$

magnetic hysteresis loop is also observed with a coercive field of 240 Oe. This is the first example of light-induced spin-crossover magnetism. In this case, the spontaneous magnetization is due to the ferrimagnetic ordering of niobium and iron(II) high-spin.

In the next material, we changed the ligand from 4-pyridinealdoxime to 4-bromopyridine (Fig. 26.6). The crystal structure is very similar. However, we checked this material using single-crystal analysis, and surprisingly, this material has two types of crystal structure. One of them is plus, the other is minus, and my student picked up many of these single crystals, about 200 crystals, and checked each of them. You can see that this material has a chiral structure.

In such a material, we can expect a new interesting phenomenon, i.e., coupling between chirality and photomagnetism (Fig. 26.7). This material is a chiral photomagnet. In such a chiral photomagnet, we expect several types of new phenomena. For example, optical control of magnetization-induced second-harmonic generation, the Magnetization-induced second harmonic generation (MSHG) effect, or optical control of the magneto-chiral dichroism behavior. Since this is the first example of a chiral photomagnet, we tried to measure these phenomena of MSHG and magneto-chiral dichroism (MChD).

Before moving on, it should be stated that we have previously reported magnetization-induced second-harmonic generation in various materials (Fig. 26.8) [13–19]. We have been studying this behavior for 15 years. Basically, in the case of magnetic materials, second-harmonic generation principally cannot be observed because the crystal structure of the usual magnetic materials are centrosymmetric. In such a case, second-harmonic generation is forbidden. But, chemists can prepare non-centrosymmetric crystal-structured materials using a molecule-based

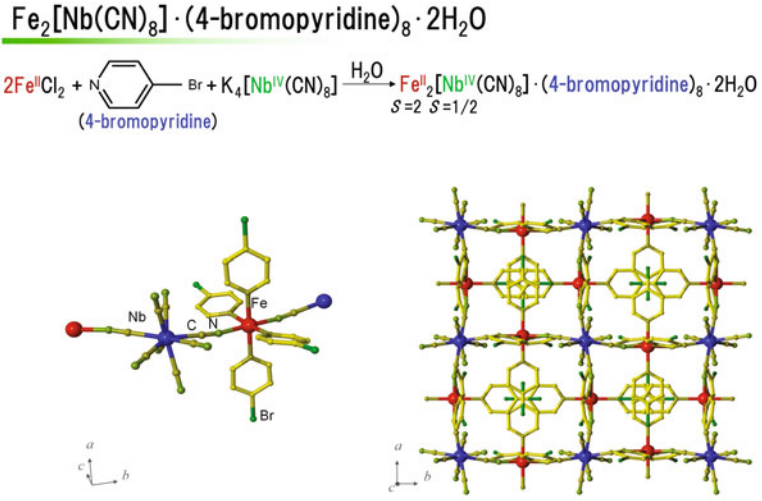

Fig. 26.6 Crystal structure of $Fe_2[Nb(CN)_8] \cdot (4\text{-bromopyridine})_8 \cdot 2H_2O$

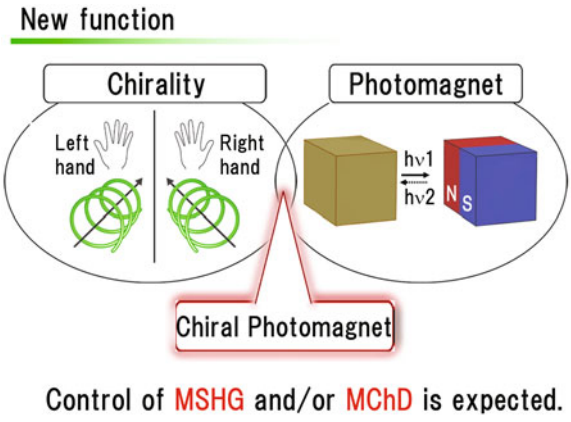

Fig. 26.7 Concept of combining chirality and photomagnetism to exhibit new functionalities such as control of MSHG and MChD by light

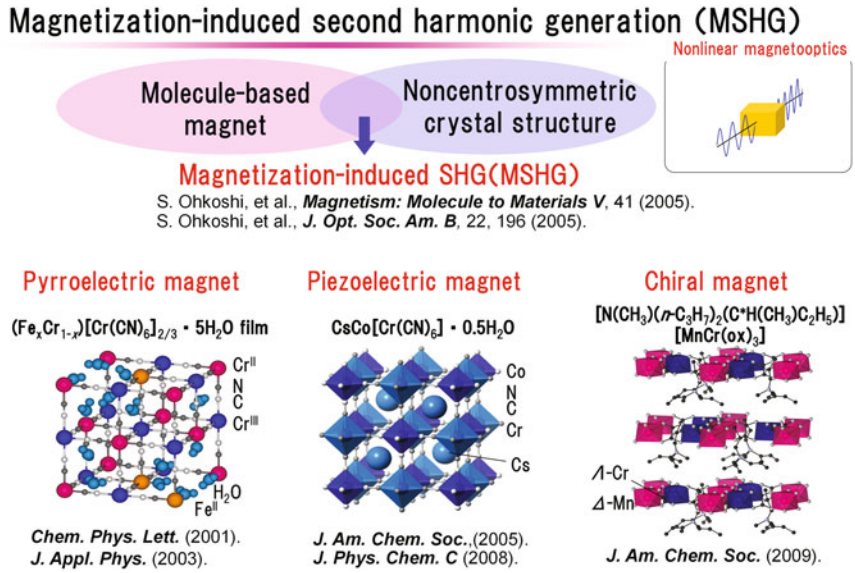

Fig. 26.8 Background researchs on magnetization-induced second-harmonic generation in molecule-based magnets with non-centrosymmetric crystal structures

magnet. Here are some examples that we have reported. In such materials, we observed magnetization-induced second-harmonic generation in a pyroelectric magnet, a piezoelectric magnet, and a chiral magnet.

26.3 Chiral Photomagnet

WWe studied the magnetic and optical properties of the chiral material, $Fe_2[Nb(CN)_8] \cdot (4\text{-bromopyridine})_8 \cdot 2H_2O$ (Fig. 26.9), e.g., the magnetic properties of this material. This material also exhibits spin-crossover behavior with a small hysteresis (Fig. 26.10). At the same time, we measured second-harmonic generation of this material because both the high-temperature phase and the low-temperature phase have non-centrosymmetric chiral-crystal structures.

First, we measured second-harmonic generation of this material at room temperature. Second-harmonic intensity is not so strong, and with decreasing temperature, the intensity increased with hysteresis, and with increasing temperature second

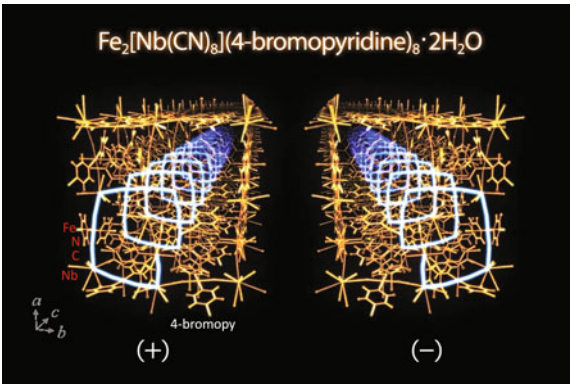

Fig. 26.9 Chiral crystal structure of $Fe_2[Nb(CN)_8] \cdot (4\text{-bromopyridine})_8 \cdot 2H_2O$

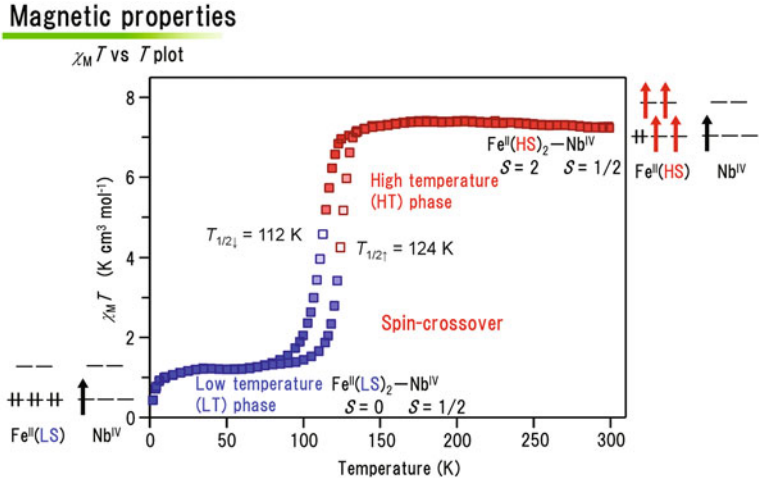

Fig. 26.10 Spin-crossover phenomenon in $Fe_2[Nb(CN)_8] \cdot (4\text{-bromopyridine})_8 \cdot 2H_2O$ observed by magnetic measurements

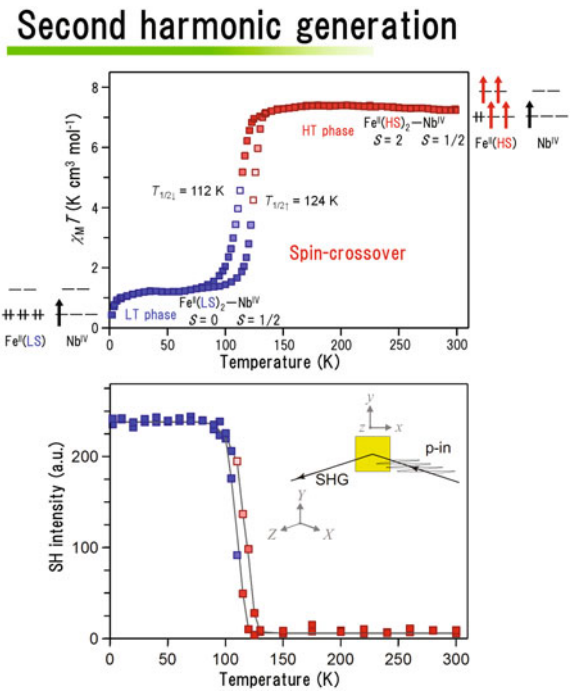

Fig. 26.11 Spin-crossover phenomenon observed in $Fe_2[Nb(CN)_8] \cdot (4\text{-bromopyridine})_8 \cdot 2H_2O$ by magnetic measurements (*upper*) and second-harmonic generation (SHG) (*lower*)

harmonic generation (SHG) intensity recovered to the original level (Fig. 26.11). In the present system, the high-temperature phase has a tetragonal structure with light color, but the low-temperature phase has an orthorhombic crystal structure and possesses deep color. Therefore, from the Kleinman's rule, the high-temperature phase shows weak second-harmonic generation, and the low-temperature phase exhibits strong second-harmonic generation.

Next, we checked the photomagnetic property of this material (Fig. 26.12). This material also exhibits photomagnetization with a Curie temperature of 15 K. This is caused by 473-nm light irradiation. Then, another light, a 785-nm light, was irradiated onto the sample. We observed a decrease of magnetization and Curie temperature. This phase is clearly a different phase because the Curie temperature is different. We named the first phase photo-induced phase I and the second phase photo-induced phase II. Before light-irradiation the material is in the low temperature phase. Photo-induced phase I and photo-induced phase II can be reversibly changed by irradiating with the two types of light sources (Fig. 26.13).

A magnetic hysteresis loop is also observed in the magnetization versus field, and the reversible change is observed by the irradiation of two different types of light (Figs. 26.14 and 26.15). The mechanism is shown in Fig. 26.16. Before light-irradiation, it is in the low-temperature phase, and by the light-irradiation, through the excited states, $^1A_1$ changes to $^5T_2$. This is the high-spin state. Conversely,

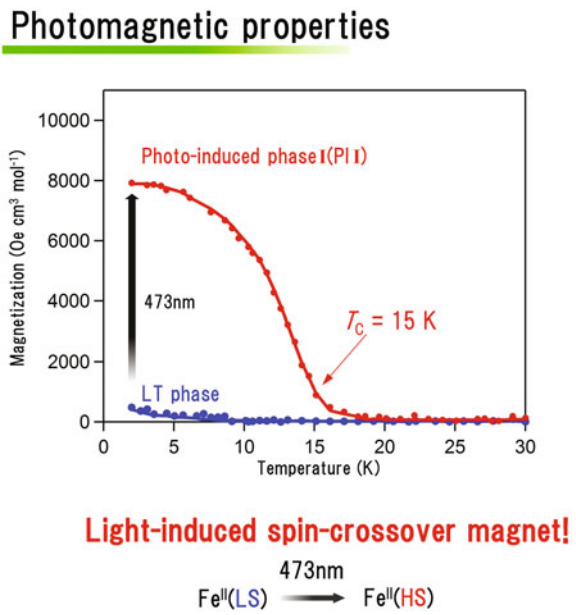

Fig. 26.12 Light-induced spin-crossover magnetization in $Fe_2[Nb(CN)_8] \cdot (4\text{-bromopyridine})_8 \cdot 2H_2O$

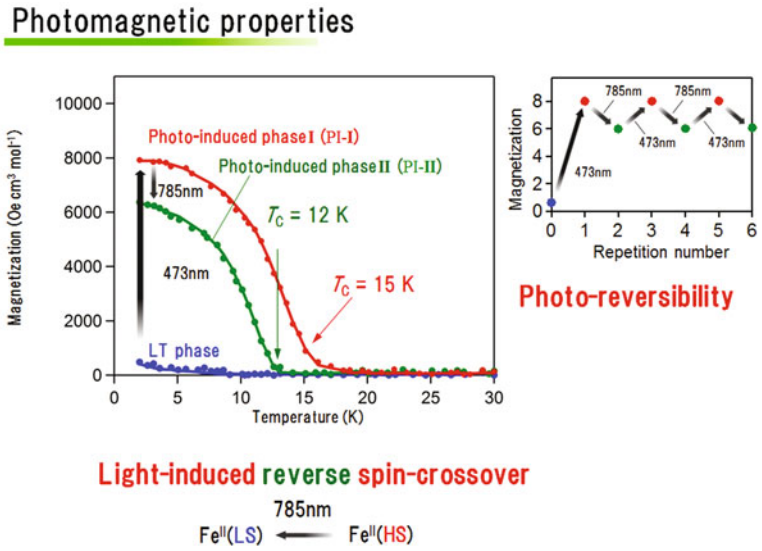

Fig. 26.13 Light-induced reverse spin-crossover magnetization in $Fe_2[Nb(CN)_8] \cdot (4\text{-bromopyridine})_8 \cdot 2H_2O$ with photo-reversibility

this high-spin state excited by the 785-nm light returns to the original low-spin state. This is reversible photo-induced spin-crossover.

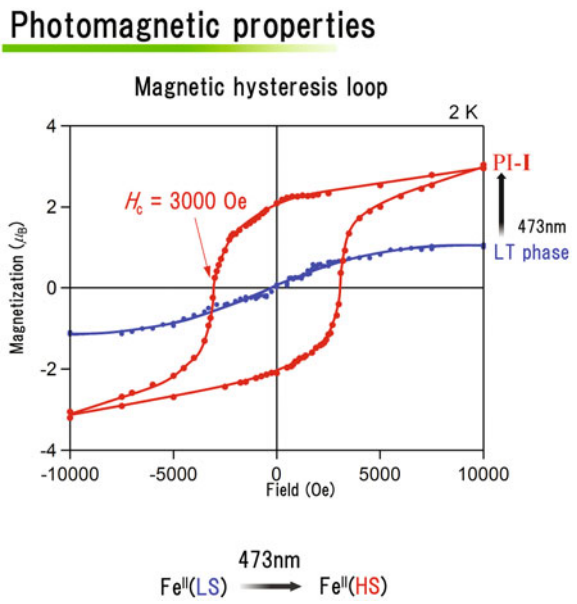

Fig. 26.14 Magnetic hysteresis of $Fe_2[Nb(CN)_8] \cdot (4\text{-bromopyridine})_8 \cdot 2H_2O$ by light-induced spin-crossover

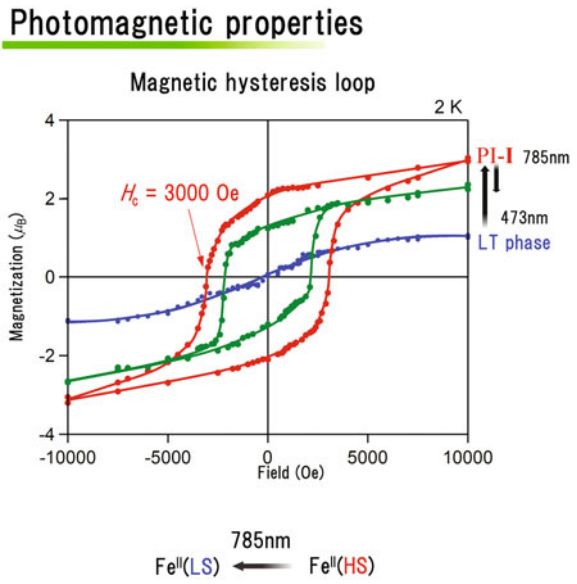

Fig. 26.15 Magnetic hysteresis of $Fe_2[Nb(CN)_8] \cdot (4\text{-bromopyridine})_8 \cdot 2H_2O$ by light-induced reverse spin-crossover

In this state, the iron site is bridged by the niobium ion, and niobium is $S = 1/2$. After light-irradiation, this effect occurs. High-spin iron and niobium leads to ferromagnetic ordering. The superexchange interaction is remarkably high, i.e., $-5.2\ cm^{-1}$. The reverse effect is also observed.

So, the low-temperature phase changes to photo-induced phase I, and then, to photo-induced phase II. We conducted measurements of various optical properties

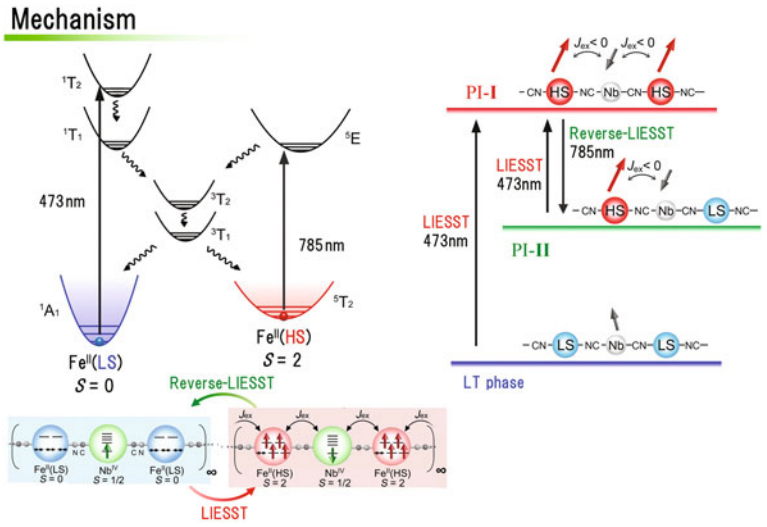

Fig. 26.16 Mechanism of light-induced spin state trapping (LIESST) and reverse LIESST effect in $Fe_2[Nb(CN)_8] \cdot (4\text{-bromopyridine})_8 \cdot 2H_2O$

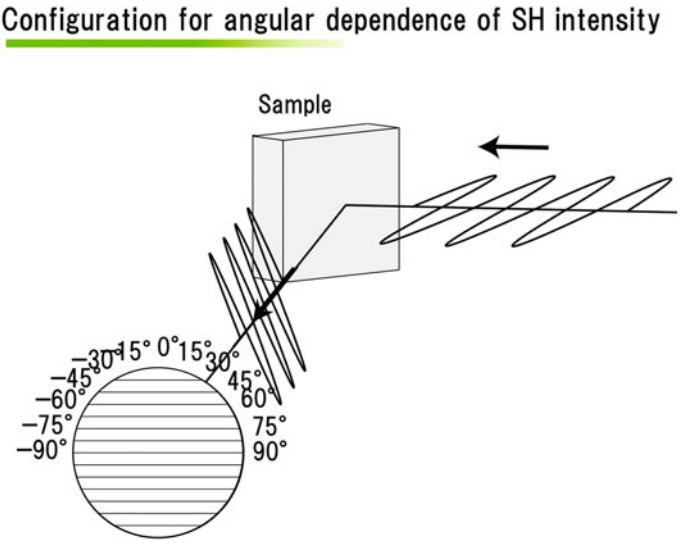

Fig. 26.17 Measurement method of angular dependence of SH intensity

and found that half of the high-spin iron is converted to low-spin iron from photo-induced phase I to photo-induced phase II. Unfortunately, this photo-induced phase I cannot be converted completely to the low-spin state and stops at an intermediate state, with a ratio of high-spin and low-spin of one-to-one. The photo-induced phase I and photo-induced phase II are reversible through light irradiation.

We measured second-harmonic generation of this photo-induced magnetization behavior using a simple optical-coordinate polarizer (Fig. 26.17). We measured the low-temperature phase, and also under light irradiation. As for low temperature phase, p-in light is irradiated onto the crystal, and then vertical second-harmonic-generation light is observed, as shown in the angle dependence of SH intensity (Fig. 26.18). By irradiation of 473-nm light, the direction of second-harmonic intensity is opposite. The minimum is at 0°. This means that horizontal second-harmonic-generation light is radiated from this sample. Furthermore, with 785-nm light, a maximum SH intensity is observed at 0° and returns to vertical SH light. Between these two phases, the reversible change of the polarization plane of SH light switches by almost 90°, without ellipticity.

vFigure 26.19 shows tensor analysis to understand the origin of the 90° switching by light irradiation. This is a very complicated analysis, but here shown is the simple explanation. After light-irradiation, photo-induced phase I and photo-induced phase II reversibly switch. Comparing the tensors of these two phases, the magnetic term shown with red circles is dominant in photo-induced phase I, and the crystal term shown with green circles is dominant in photo-induced phase II. This difference changes the polarization plane of the second-harmonic generation.

Second-harmonic intensity is expressed by the crystal term and the magnetic term (Fig. 26.20). When the crystal term is stronger than the magnetic term, the maximum of second-harmonic intensity is at 0°. When the magnetic term overcomes the crystal term, the minimum is at 0°. This is a simple explanation of this phenomenon.

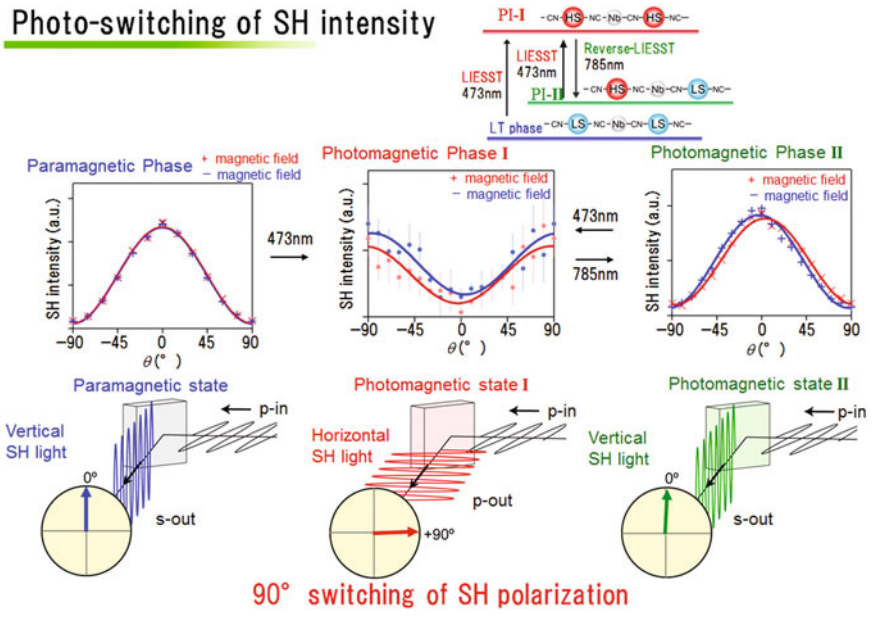

Fig. 26.18 Photo-switching phenomenon of SH polarization in $Fe_2[Nb(CN)_8] \cdot (4\text{-bromopyridine})_8 \cdot 2H_2O$

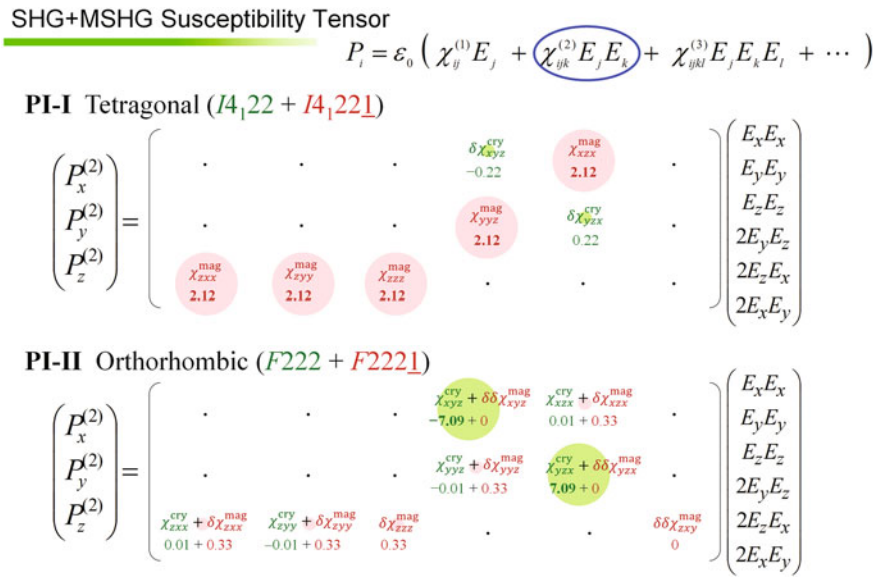

Fig. 26.19 SHG and MSHG susceptibility tensors of the photo-induced phase I and photo-induced phase II of $Fe_2[Nb(CN)_8] \cdot (4\text{-bromopyridine})_8 \cdot 2H_2O$

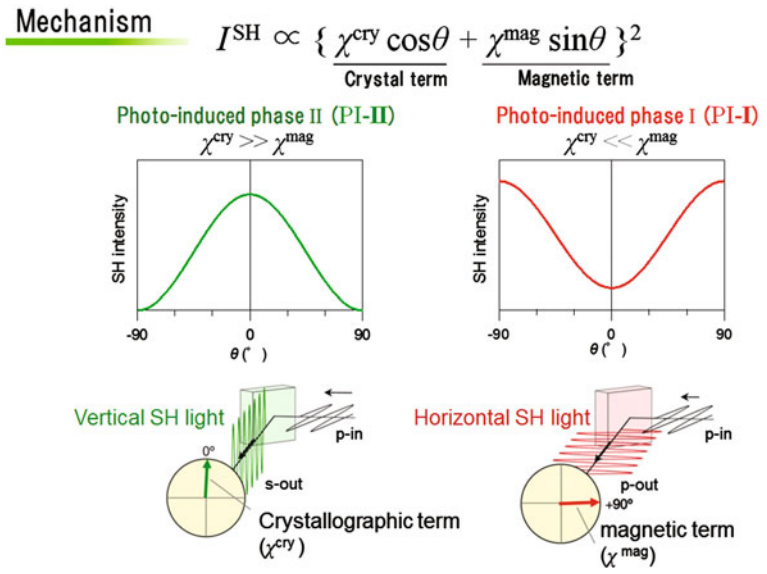

Fig. 26.20 Mechanism of 90° optical switching of the SH polarization in $Fe_2[Nb(CN)_8] \cdot (4\text{-bromopyridine})_8 \cdot 2H_2O$

Here is the future work that we are considering: Not only 90° switching, but also switching of intermediate angles is possible by controlling the light intensity or magnetization (Fig. 26.21). This means that this crystal is applicable not only in a binary system but also in denary or n-ary systems. For example, n-ary optical recording memory could be possible (Fig. 26.22).

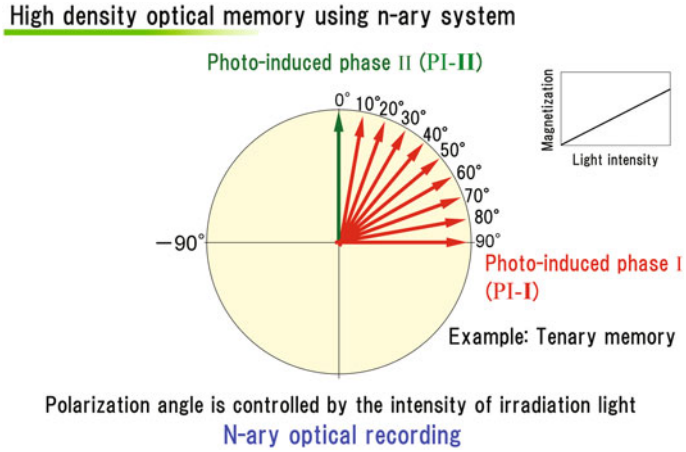

Fig. 26.21 Possible application of the observed optical-switching phenomenon as a high-density optical memory using n-ary system

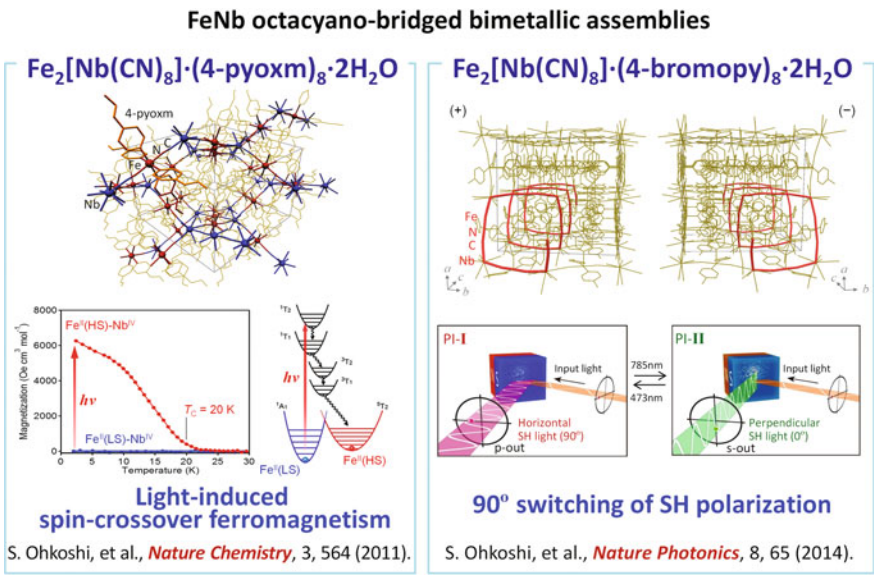

Fig. 26.22 Summary of "Magneto-optical functionalities in cyano-bridged bimetal assemblies and metal oxide nanomaterials"

References

1. S. Ohkoshi, H. Tokoro, Acc. Chem. Res. **45**, 1749–1758 (2012)
2. S. Ohkoshi, K. Imoto, Y. Tsunobuchi, S. Takano, H. Tokoro, Nat. Chem. **3**, 564–569 (2011)
3. S. Ohkoshi, S. Takano, K. Imoto, M. Yoshikiyo, A. Namai, H. Tokoro, Nat. Photonics **8**, 65–71 (2014)
4. T. Mahfoud, G. Molnar, S. Bonhommeau, S. Cobo, L. Salmon, P. Demont, H. Tokoro, S. Ohkoshi, K. Boukheddaden, A. Bousseksou, J. Am. Chem. Soc. **131**, 15049–15054 (2009)
5. E. Pardo, C. Train, G. Gontard, K. Boubekeur, O. Fabelo, H. Liu, B. Dkhil, F. Lloret, K. Nakagawa, H. Tokoro, S. Ohkoshi, M. Verdaguer, J. Am. Chem. Soc. **133**, 15328–15331 (2011)
6. S. Ohkoshi, K. Arai, Y. Sato, K. Hashimoto, Nat. Mater. **3**, 857–861 (2004)
7. S. Ohkoshi, Y. Abe, A. Fujishima, K. Hashimoto, Phys. Rev. Lett. **82**, 1285–1288 (1999)
8. S. Ohkoshi, A. Fujishima, K. Hashimoto, J. Am. Chem. Soc. **120**, 5349–5350 (1998)
9. E. Pardo, C. Train, H. Liu, L.M. Chamoreau, B. Dhkil, K. Boubekeur, F. Lloret, K. Nakatani, H. Tokoro, S. Ohkoshi, M. Verdaguer, Angew. Chem. Int. Ed. **51**, 8356–8360 (2012)
10. S. Ohkoshi, Y. Tsunobuchi, T. Matsuda, K. Hashimoto, A. Namai, F. Hakoe, H. Tokoro, Nat. Chem. **2**, 539–545 (2010)
11. A. Namai, M. Yoshikiyo, K. Yamada, S. Sakurai, T. Goto, T. Yoshida, T. Miyazaki, M. Nakajima, T. Suemoto, H. Tokoro, S. Ohkoshi, Nat. Commun. **3**, 1035 (2012)
12. A. Namai, S. Sakurai, M. Nakajima, T. Suemoto, K. Matsumoto, M. Goto, S. Sasaki, S. Ohkoshi, J. Am. Chem. Soc. **131**, 1170–1173 (2009)
13. K. Inoue, S. Ohkoshi, H. Imai, in *Magnetism: Molecules to Materials V*, ed. By J.S. Miller, M. Drillon (Wiley-VCH, Weinheim, 2005) (Chapter 2)
14. S. Ohkoshi, J. Shimura, K. Ikeda, K. Hashimoto, J. Opt. Soc. Am. B **22**, 196–203 (2005)
15. K. Ikeda, S. Ohkoshi, K. Hashimoto, Chem. Phys. Lett. **349**, 371–375 (2001)
16. K. Ikeda, S. Ohkoshi, K. Hashimoto, J. Appl. Phys. **93**, 1371–1375 (2003)
17. T. Nuida, T. Matsuda, H. Tokoro, S. Sakurai, K. Hashimoto, S. Ohkoshi, J. Am. Chem. Soc. **127**, 11604–11605 (2005)
18. S. Ohkoshi, S. Saito, T. Matsuda, T. Nuida, H. Tokoro, J. Phys. Chem. C **112**, 13095–13098 (2008)
19. C. Train, T. Nuida, R. Gheorghe, M. Gruselle, S. Ohkoshi, J. Am. Chem. Soc. **131**, 16838–16843 (2009)